

Breakdown of Herring's processes in cubic semiconductors for subterahertz longitudinal acoustic phonons

Maxime Markov, Jelena Sjakste, and Nathalie Vast


Laboratoire des Solides Irradiés (LSI), École Polytechnique–CEA/DRF/IRAMIS–CNRS UMR 7642, 91128 Palaiseau cédex, France

Romain Legrand and Bernard Perrin

Institut de Nanosciences de Paris (INSP), Sorbonne Université, CNRS UMR 7588, Case 840, 4 place Jussieu, 75252 Paris Cedex 05, France

Lorenzo Paulatto*

Institut de Minéralogie, de Physique des Matériaux et de Cosmochimie (IMPMC), Sorbonne Université, CNRS UMR 7590, IRD UMR 206, Case 115, 4 place Jussieu, 75252 Paris Cedex 05, France

 (Received 4 August 2018; revised manuscript received 21 November 2018; published 10 December 2018)

In the present work we explain the anomalous behavior of the attenuation of the longitudinal acoustic phonon in GaAs as a function of the phonon energy ω in the subterahertz domain. These attenuations along the [100] direction show a plateau between 0.6 and 1 GHz at low temperatures. We found an excellent agreement between measurements performed by some of us, and new *ab initio* calculations of third-order anharmonic processes. The formation of the plateau is explained by the competition between different phonon-phonon scattering processes such as Herring's mechanism, which dominates at low frequencies, saturates, and disappears. The plateau is shown to be determined by the phononic final-state phase space available at a given temperature. We predict that a change of scattering mechanism should also show up in the attenuation of silicon around 1.2–1.7 THz, and argue that the attenuation plateau is a general feature of cubic semiconductors.

DOI: [10.1103/PhysRevB.98.245201](https://doi.org/10.1103/PhysRevB.98.245201)

I. INTRODUCTION

Many efforts have been devoted to the measurement of the absorption of ultrasonic waves with frequencies below a few gigahertz [1]. The results have been discussed in the framework of the Landau-Rumer or Akhiezer theories according to the frequency and temperature ranges in which they have been performed [2–7]. On the other hand, high frequency phonon lifetimes are actively studied nowadays in relation to thermal and thermoelectric transports, both experimentally [8,9] and by computer simulations [10–15].

However, there are only very few studies about the damping of subterahertz acoustic waves although a full understanding of the attenuation of these waves is becoming crucial in several respects: (i) Efforts are devoted today to develop non-destructive methods for phonon imaging of deeply embedded nanostructures using picosecond acoustics, potentially very important for microelectronics [16]. It is thus important to know the absorption length of short acoustic pulses in standard semiconducting materials (silicon, germanium, sapphire, GaAs) commonly used for microelectronics. (ii) Quantum optomechanics can play a major role in quantum information: the challenge is to use resonators with higher frequencies (tens of gigahertz, instead of the current threshold of some hundreds of megahertz), which would allow one to observe the quantum regime at higher temperatures [17]. Then, a key problem is the limitation of the quality factor of such resonators due to

the intrinsic phonon-phonon interaction intervening at higher temperatures [18,19].

Attenuation of subterahertz acoustic waves can be studied by the so-called “picosecond ultrasonic technique” [20]. In such experiments, either short acoustic pulses with a broad spectrum ranging from a few tens of gigahertz up to hundreds of gigahertz, or monochromatic coherent acoustic waves up to a few terahertz, can be generated and detected by metallic films, quantum wells, or semiconducting superlattices [21–23]. The attenuation of these propagating sound waves can be measured over a large temperature range using samples with thickness going from a few micrometers up to millimetric size [23–27]. At low temperature in pure crystals, the damping of acoustic waves above 10 GHz is mainly due to three-phonon interactions, which corresponds to the so-called Landau-Rumer (LR) regime. Under such conditions, one can get access to accurate experimental information about lifetimes of individual longitudinal acoustic (LA) phonons. At higher temperatures, the LR regime holds only for higher frequencies (above 100 GHz). At lower frequencies, the three-phonon perturbation description breaks down and the system crosses into the Akhiezer regime, where the collective response of phonon populations under the effect of the strain field induced by the acoustic wave has to be taken into account. In the intermediate regime between the LR and Akhiezer ones, the finite lifetime of phonons interacting with the exciting longitudinal acoustic wave should also be taken into account.

In the LR regime, the interaction of three phonons is the main mechanism of the phonon decay [28]. For a longitudinal

*lorenzo.paulatto@sorbonne-universite.fr

acoustic wave propagating in an anisotropic crystal, Herring has pointed out a dominant three-phonon coalescence mechanism involving the scattering of the excited longitudinal acoustic wave by a slow transverse phonon into a fast transverse phonon: $\omega_{LA} + \omega_{TA_s} \rightarrow \omega_{TA_f}$, where ω are the phonon frequencies, LA refers to the longitudinal branch, and TA_s , TA_f to the transverse branches with, respectively, the lowest and highest sound velocities [29]. Herring's processes are dominant because they allow the coupling of low-energy longitudinal phonons close to the Γ point, to transverse phonons which have a much higher wave vector \mathbf{q} and, thus, a large density of states. Using symmetry arguments, Herring predicted that the contribution of this process should be proportional to $\omega^2 T^3$ in cubic crystals, where T is the temperature. However, this dependence only holds in a very limited frequency and temperature domain [30] and no general theoretical statement has been made beyond these limits yet. Recent experimental measurements on the absorption of subterahertz longitudinal waves made by some of us in gallium arsenide [27] showed that after a steep increase, the attenuation exhibits an unexpected plateau as a function of the excitation frequency in the 700 GHz to 1 THz range. This plateau has been ascribed, on the basis of strong hypotheses, to a breakdown of the Herring processes [27].

In this paper, we consider acoustic waves of frequency up to 1 or 2 THz, at temperatures between 50 and 300 K for silicon, and down to 2 K for gallium arsenide. We study acoustic phonon attenuation in GaAs and Si by means of *ab initio* calculations based on the density functional perturbation theory [31]. We show that the attenuation plateau observed experimentally [27] in GaAs can be fully reproduced by *ab initio* calculations, and can be explained by the density of final states available for different phonon-phonon scattering processes. More precisely, the plateau is explained by the rapid decrease of the probability of Herring's processes in the 700 GHz to 1 THz range, whereas the probability of other phonon-phonon scattering processes is found to increase. Moreover, we predict that a similar plateau in the attenuation of acoustic phonons should be observed in silicon around 1.2–1.7 THz.

The paper is organized as follows: first, we present our *ab initio* method to compute phonon attenuation due to three-phonon interaction, and provide technical details which concern in particular the convergence of phonon lifetimes. Secondly, we present our calculations for the attenuation of acoustic phonons in GaAs, comparing with experimental data. We discuss the origin of the attenuation plateau found both theoretically and experimentally and examine the roles of the joint density of final states available for different phonon-phonon scattering processes, in particular for Herring's processes. The role of the matrix elements of the phonon-phonon interaction is investigated. In the fourth and fifth sections, we present our predictions for the attenuation in silicon, we justify our conclusion that Herring's breakdown is general to cubic semiconductors, and discuss the conditions of its observation. Finally, we discuss the applicability of the long-wavelength approximation for the anharmonic coupling coefficients which we express in terms of third-order elastic constants [32–34].

II. METHOD

The computational method to obtain fully *ab initio* the matrix elements of the phonon-phonon interaction has been described in detail in Ref. [31], and in papers cited therein. For the sake of completeness, we review the theory involved using the compact notation of Ref. [14]. To first order in perturbation theory, the intrinsic phonon-phonon interaction is described by one single Feynmann's diagram (the "bubble" diagram) [35]. This diagram describes both the decay (fission) process, where the initial phonon decays into two phonons, and the coalescence (fusion) process, where the phonon is scattered by another one to create a new phonon. In both kinds of processes, the total energy and the crystal momentum have to be conserved, the latter modulo a vector \mathbf{G} of the reciprocal lattice because of periodic boundary conditions.

Identifying the phonon by its wave vector \mathbf{q} and branch index j , and referring to the phonon energy $\omega_{\mathbf{q},j}$ and Bose-Einstein occupation $n_{\mathbf{q},j}$, we define the inverse of the phonon lifetime $\tau_{\mathbf{q},j}^{-1}$ as a sum in the reciprocal space [35,36]:

$$\begin{aligned} (\tau_{\mathbf{q},j}^{-1}) &= \frac{\pi}{\hbar N_0} \sum_{\mathbf{q}',j',\mathbf{q}'',j''} |V^{(3)}(\mathbf{q},j,\mathbf{q}',j',\mathbf{q}'',j'')|^2 \\ &\times [(1+n_{\mathbf{q}',j'}+n_{\mathbf{q}'',j''})\delta(\hbar\omega_{\mathbf{q},j}-\hbar\omega_{\mathbf{q}',j'}-\hbar\omega_{\mathbf{q}'',j''}) \\ &+ 2(n_{\mathbf{q}',j'}-n_{\mathbf{q}'',j''})\delta(\hbar\omega_{\mathbf{q},j}+\hbar\omega_{\mathbf{q}',j'}-\hbar\omega_{\mathbf{q}'',j''})]. \end{aligned} \quad (1)$$

In this equation, we have introduced $V^{(3)}(\mathbf{q},j,\mathbf{q}',j',\mathbf{q}'',j'')$, the matrix elements of the phonon-phonon interaction that are closely related to the third-order derivatives of the total electronic energy, calculated with respect to three phonons. We compute them fully *ab initio*, using density functional perturbation theory [37] and the "2n + 1" theorem [38–40]. The conservation of momentum is imposed by requiring that $\mathbf{q}'' = -(\mathbf{q} + \mathbf{q}')$. In our case, \mathbf{q} is the momentum of the initial acoustic wave (phonon) for which the attenuation is calculated, \mathbf{q}' runs on a regular grid of N_0 points in the whole Brillouin zone, and \mathbf{q}'' is fixed by momentum conservation.

The first term of Eq. (1) describes decay processes, while the second one describes coalescence processes. Because of the magnitude of the Bose-Einstein occupation terms, decay processes usually dominate. However, the conservation of energy [expressed by the first Dirac δ function in Eq. (1)] requires that the two created phonons (\mathbf{q}',j') and (\mathbf{q}'',j'') have values of the energy lower than that of the initial phonon. As a consequence, for low-energy initial acoustic phonons, there tends to be no suitable final states for decay, so that the contribution of decay terms to the sum of Eq. (1) is negligible. On the other hand, the second term of Eq. (1) describes coalescence processes whose contribution to the sum of Eq. (1) is small for optical phonons, but turns out to dominate for low-energy acoustic phonons, as predicted by Herring, but with limitations that are the subject of the following sections.

The attenuation of ultrasound waves is related to the acoustic field amplitude by the following relation:

$$A_z(T) = A_0 e^{-\alpha(T)z}, \quad (2)$$

where A_z is the measured amplitude, A_0 is the amplitude of the generated pulse, z is the distance from the pulse source, and α is the attenuation. The attenuation is inversely proportional to the phonon lifetime and its group velocity, i.e., to the derivative of the phonon frequency with respect to the wave vector [41] $\mathbf{v}_{\mathbf{q},j} = \nabla_{\mathbf{q}}\omega_{\mathbf{q},j}$. The attenuation reads

$$\alpha_{\mathbf{q},j} = \frac{1}{2|\mathbf{v}_{\mathbf{q},j}|\tau_{\mathbf{q},j}}. \quad (3)$$

In order to understand which decay mechanisms contribute to the attenuation, we will study the temperature-dependent joint phonon density of states (T-JDOS) which gives information about the phase space available for scattering processes involving a specific phonon (\mathbf{q}, j) . In its most general form the definition of the T-JDOS, $\theta_{\mathbf{q},j}$, is based on Eq. (1), with matrix elements set to a constant value:

$$\begin{aligned} \theta_{\mathbf{q},j} = & \frac{\pi}{\hbar N_0} \sum_{\mathbf{q}',j',j''} \\ & \times [(1 + n_{\mathbf{q}',j'} + n_{\mathbf{q}'',j''})\delta(\hbar\omega_{\mathbf{q},j} - \hbar\omega_{\mathbf{q}',j'} - \hbar\omega_{\mathbf{q}'',j''}) \\ & + 2(n_{\mathbf{q}',j'} - n_{\mathbf{q}'',j''})\delta(\hbar\omega_{\mathbf{q},j} + \hbar\omega_{\mathbf{q}',j'} - \hbar\omega_{\mathbf{q}'',j''})]. \end{aligned} \quad (4)$$

If we only take the first line of the definition, we get the decay-specific T-JDOS ($\theta_{\mathbf{q},j}^D$), while the second line would give the coalescence part ($\theta_{\mathbf{q},j}^C$). Furthermore, we can restrict the latter to processes that are described by Herring's mechanism: a coalescence process where a LA phonon combines with a slow TA phonon to form a fast TA. In practice, this can be done by imposing that all of the phonons involved are acoustic ones, that (\mathbf{q}, j) is longitudinal, and that $\omega_{\mathbf{q}',j'} \leq \omega_{\mathbf{q}'',j''}$. With these constraints, we get the Herring contribution to the T-JDOS ($\theta_{\mathbf{q},j}^H$). We will see in Sec. IV D 1 up to which point the Herring T-JDOS is a good approximation for the full decay mechanism.

III. COMPUTATIONAL METHOD

A. Calculation details

Calculations were performed with the QUANTUM-ESPRESSO code [42,43] using the LDA-PZ [44] exchange and correlation functional. This functional is less popular than the Perdew-Burke-Ernzerhof [45] one. It gives, however, a theoretical lattice parameter close to the experimental one in cubic semiconductors, which is extremely important to obtain a good description of the phonon dispersion. For silicon, we have used pseudopotentials from the Fritz-Haber-Institut library [46]. The pseudopotentials for gallium and arsenic were generated with the FHIPP code [46], and are the same ones as those used in Refs. [47–49].

We constructed a crystal unit cell and relaxed it to the theoretical lattice parameter, which was found to be 10.591 bohrs for GaAs and 10.167 bohrs for Si. The use of the experimental lattice parameters for both GaAs and Si was found to yield very little difference in the results. The Kohn-Sham set of equations was integrated in the reciprocal space over a shifted Monkhorst-Pack [50] grid of $12 \times 12 \times 12$ (GaAs) or $8 \times 8 \times 8$ (Si) \mathbf{k} points. The use of a grid shifted from the

Γ point was crucial to obtain properly converged results in GaAs, especially in the calculation of effective charges from the linear response theory. We used a kinetic cutoff energy of 45 Ry, for which phonon frequencies at the Γ point were converged within 1 cm^{-1} . For the present application, we decided to converge very strictly all parameters, as the cost of the *ab initio* calculation using the “ $2n + 1$ ” theorem is negligible with respect to the integration over the Brillouin zone in Eq. (1).

B. Convergence of the inverse lifetime

Indeed, Eq. (1) includes two Dirac delta functions that enforce the conservation of energy. To make the integration feasible, these delta distributions are replaced by Gaussian functions of finite width, under the condition that the chosen width is smaller than energy differences of phonons involved in the process. In order to obtain good quality results, the sum over \mathbf{q} points of the reciprocal space must be done over a grid which is sufficiently fine to sample a significant number of nonzero scattering processes. However, the number of points increases rapidly as we tackle low-temperature and low-energy phonons, because the finite width of the Gaussian has to be reduced to maintain the computational accuracy.

Such a fine grid cannot be directly computed from density functional perturbation theory. We thus exploit the fact that phonon dynamical matrices and phonon-phonon coupling matrices change smoothly in reciprocal space, and use Fourier transform to pass from a relatively coarse grid of points, computed directly *ab initio*, to short-ranged two- and three-body force constants in real space. The latter quantities are interpolated in real space, assuming that they are short ranged. A second Fourier transform, back to the reciprocal space, allows one to compute phonon dynamical matrices and phonon-phonon coupling matrices at any \mathbf{q} on an ultrafine grid. Details of the interpolation scheme can be found in Ref. [31].

In the present application, we have computed the phonon dynamical matrices *ab initio* on an initial $8 \times 8 \times 8$ \mathbf{q} -point grid in the reciprocal space, and the phonon-phonon coupling matrices on a $4 \times 4 \times 4$ \mathbf{q} -point grid. To evaluate the integral of Eq. (1) the code does not employ symmetry operations to reduce the grid size, hence a uniform Γ -centered grid is not the best choice for the integration, as a large number of equivalent points would be included in the integral. We found instead that the use of a randomly shifted grid, which is incommensurate to any symmetry operation, yields the fastest convergence. Although symmetry is formally broken, we checked that it is numerically recovered at convergence. All of the phonon lifetime calculations have been performed with a grid containing as many as $199 \times 199 \times 199$ points. The finite smearing was chosen to be 0.2 cm^{-1} for GaAs and 0.5 cm^{-1} for Si, respectively. Reducing the grid size to $39 \times 39 \times 39$ \mathbf{q} -point was proven to be sufficient in almost every case, when used with a large smearing value of 2 cm^{-1} (66 GHz). It was, however, insufficient to reproduce the correct behavior of the attenuation when the initial-phonon frequency was smaller than 100 GHz.

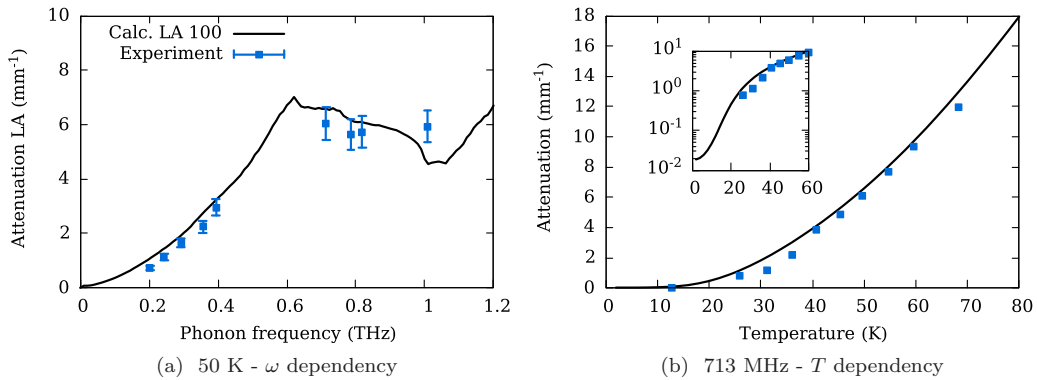


FIG. 1. Phonon attenuation in GaAs: comparison of calculations with experiments (a) at fixed temperature (50 K) as a function of phonon frequency along the [100] direction and (b) at fixed energy ($\omega = 713$ GHz) as a function of temperature. The inset shows data on a logarithmic scale for α to magnify the low-temperature behavior. Similar pictures for all of the points measured in Ref. [27] are provided in the Supplemental Material [52].

IV. RESULTS FOR GALLIUM ARSENIDE

A. Attenuation of LA phonons along [100]

We focus on the case for which we are able to directly compare experimental results and calculations: the longitudinal phonon branch along the [100] direction. As shown in Fig. 1(a), the agreement is remarkable. Not only does the calculation correctly reproduce the qualitative behavior of $\alpha(\omega)$, and the presence of the plateau between 600 GHz and 1 THz, but also the experimental and calculated absolute values of the attenuation are very close. We stress that no renormalization has been applied to the data: the values of the attenuation directly come from the *ab initio* calculations.

In Fig. 1(b), we examine the behavior of α at the fixed frequency value of 713 GHz, as a function of the temperature, and compare it with the experimental data. The low-temperature region is magnified in the inset of Fig. 2. The agreement between the *ab initio* calculations and the experimental data (starting from 20 K) is strikingly good even at very low temperature. We report in the Supplemental Material [52] the comparison for eight different frequencies, with similar conclusions.

At this point it is important to note that the experimental data correspond only to the relative change of attenuation with temperature defined by

$$\alpha(T) - \alpha(10 \text{ K}) = -\frac{1}{z} \ln \left(\frac{A_z(T)}{A_z(10 \text{ K})} \right), \quad (5)$$

where A_z is defined in Eq. (2), while the *ab initio* data is the absolute value of the attenuation given by Eq. (3).

Thus, the experimental points would eventually go exactly to zero, at zero temperature, while the theoretical data, which take into account spontaneous decay processes, have therefore a finite limit at 0 K. The extremely good agreement above approximately 30 K implies that, indeed, the experimental points can also be considered as absolute values of the sound attenuation. The behavior of the *ab initio* data displayed in Fig. 1(b) is typical of what could be expected from the temperature dependence of the inverse lifetime: a slow growth starting from a finite value at low temperature, which eventually becomes linear, in this case above 90 K (not shown).

B. Comparison of LA and TA modes and propagation directions

In Fig. 2 we extend the computation to the [111] direction, and to phonon modes which are not readily accessible by experiment.

The behavior of the computed attenuation for transverse phonons is different from that of the longitudinal one: while for the LA branch we have a very clear plateau between 600 GHz and 1 THz, for the TA branches the attenuation only shows a shoulder around 1 THz.

We also report the attenuation of LA and TA phonons along the [111] direction. None of the attenuations of the two branches has such a clear plateau as the LA phonon attenuation along the [100] direction, but we observe a change of behavior around 1 THz, where the attenuation starts to grow faster as the phonon energy increases.

At room temperature [panel (b), Fig. 2], the plateau observed for the longitudinal wave along the [100] direction moves to lower energies, around 400 GHz, and extends over a frequency range smaller than the one at 50 K. Finally, a small dip is predicted at 400 GHz for the longitudinal wave along the [111] direction as well as for the transverse waves in both [100] and [111] directions.

C. Results at cryogenic temperatures

Some measurements of the phonon attenuation in GaAs, additional to those of Ref. [27], are available in Ref. [51]. The mean-free path (MFP) of the 650 GHz LA phonon along [111] was measured at a temperature of 2 K, the reported value being 0.8 mm. At such a low temperature, the intrinsic phonon-phonon scattering is small with respect to the scattering of phonons with isotopic disorder and potentially with other lattice defects and impurities. We have simulated this MFP including only intrinsic scattering (not shown), and found a value of 40 mm. However, when we included isotopic scattering, as done in Ref. [14], the MFP was reduced to 2.7 mm, which we consider an acceptable estimation of the intrinsic MFP. Indeed, the difference between our result and the experiment of Ref. [51] is the signature of the presence of additional scattering sources in the experiment, i.e., lattice defects and surface roughness.

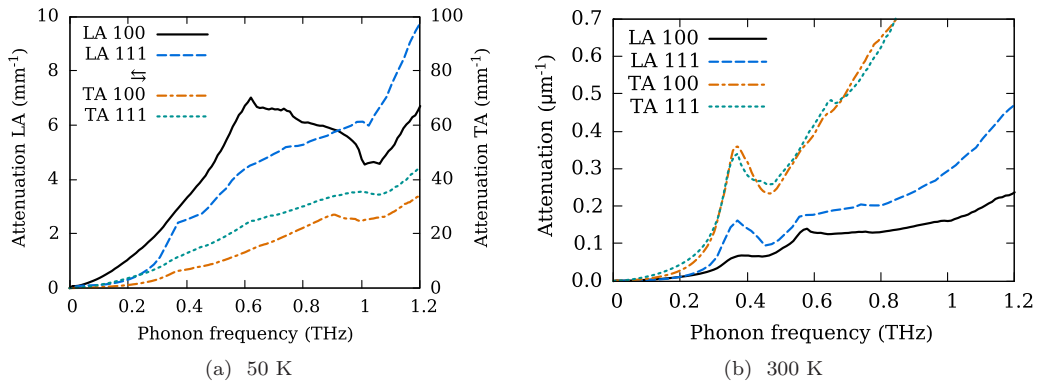


FIG. 2. GaAs. Attenuation of longitudinal and transverse phonons along the [100] and [111] directions at 50 K (left panel) and 300 K (right panel). Note the change of scale between the two temperatures (panels), as well as the different axis for the TA mode (on the right) in the left panel.

D. Discussion on the frequency dependence of the attenuation

To understand the origin of the plateau, we study whether it comes from the behavior of transition matrix elements, or whether it is a property of the phonon dispersion, modulated by the matrix elements.

1. Temperature-dependent joint density of states

We have computed the T-JDOS of Eq. (4) in the subterahertz region of the acoustic phonons in GaAs, along the [100] and [111] high-symmetry directions at two temperatures, 50 and 300 K, as well as contributions to T-JDOS from different scattering channels. We have observed that the T-JDOS is almost perfectly isotropic at the energies under consideration; furthermore, the effect of temperature is limited to a change in magnitude, both absolute and between different contributions. For these reasons, in Fig. 3, we only report the T-JDOS at 50 K and along the [100] direction, which we discuss below.

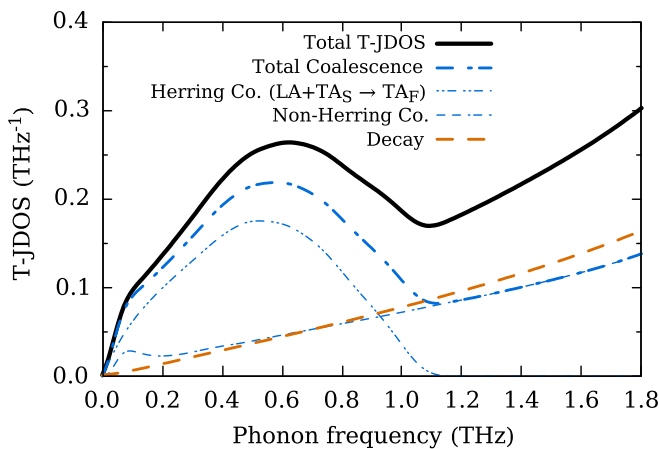


FIG. 3. Temperature-dependent joint density of states (T-JDOS) at 50 K for the LA branch of GaAs along the [100] direction. The total T-JDOS (thick black solid line) is decomposed into decay (dashed orange) and coalescence (dot-dashed blue) processes, the latter being further divided into Herring's ($LA \rightarrow TA_S + TA_F$; blue dash-dotted lines) and non-Herring's (blue long-dashed lines) processes.

As one can see from Fig. 3, for initial phonon frequencies under 1 THz, it is indeed the Herring mechanism that dominates over other phonon-phonon scattering mechanisms. However, while the contribution of other decay and coalescence events grows linearly when the frequency increases, the Herring contribution saturates around 500 GHz. At this frequency, Herring's mechanism is still contributing by more than one-half, up to two-thirds, to the total value of the T-JDOS, but it quickly loses importance until it completely dies off just beyond 1 THz. This breakdown of Herring's processes produces the change of slope in the total T-JDOS, which is the origin of the attenuation plateau experimentally observed in GaAs at low temperatures (Fig. 2 and Ref. [27]).

At 300 K (results not shown in the main text) [52], the global picture is found to be very similar, but the steepness of the non-Herring contributions is higher than at 50 K. This moves the maximum of the total T-JDOS down toward lower energies, as Herring's processes are drowned sooner by the other scattering mechanisms than at 50 K. Because the Herring contribution picks up very quickly from zero, it may appear as a short sharp peak or only as a change in the steepness of the total T-JDOS: the exact effect will depend crucially on the details of the matrix elements which govern the relative magnitude of the different mechanisms.

2. Final states for phonon scattering

On the one hand, T-JDOS plays the major role and it is the superimposition of the hill-shaped curve of the Herring mechanism and of the linear curve of the other processes, that results in the formation of the plateau. On the other hand, the matrix elements are still important: they fix the relative magnitude of scattering mechanisms and enable (prevent) the transitions which are allowed (forbidden) by symmetry, giving a much more complex shape and anisotropy of the attenuation (Fig. 2) with respect to the simple and isotropic shape of the T-JDOS.

Furthermore, the scattering processes contributing to the attenuation strongly depend on the direction because of the selection rules embedded in the matrix elements. In Fig. 4 we have decomposed the contribution to the attenuation by

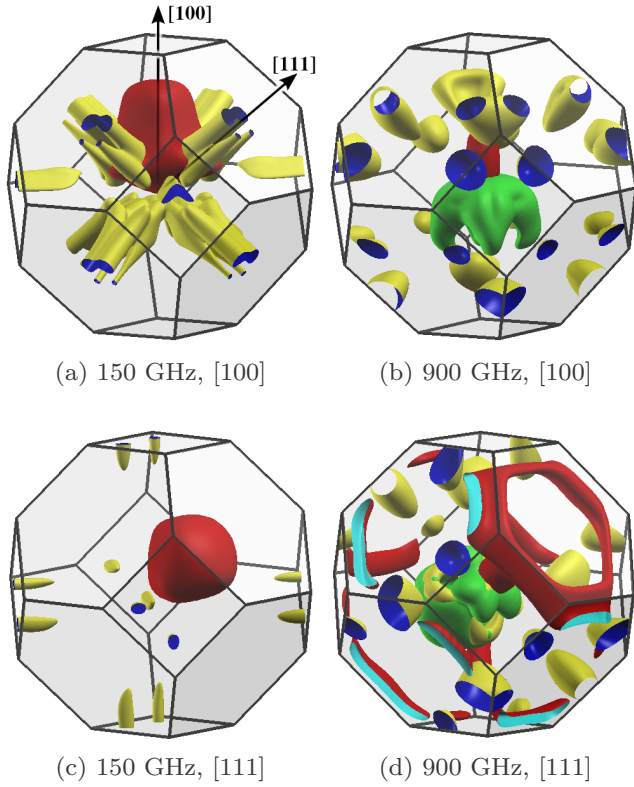


FIG. 4. GaAs at 50 K. Brillouin volume spanned by the wave vectors of the phonons involved in the scattering of LA phonons along the directions [100] [panels (a) and (b)] and [111] [panels (c) and (d)]. The initial state is either at 150 GHz [panels (a) and (c)] or at 900 GHz [panels (b) and (d)]. The volume inside the surfaces contributes 75% to the scattering events. Surface-outside/inside colors allow one to identify the final-state phonon in the following way: TA slow is yellow/blue, TA fast is red/cyan, and LA is green/magenta. The [100] direction is oriented upward.

convoluting Eq. (1) with $\delta(\mathbf{q}' - \bar{\mathbf{q}})$:

$$\begin{aligned}
 & (\tau^{\mathbf{q},j,j'}(\bar{\mathbf{q}}))^{-1} \\
 &= \frac{\pi}{\hbar N_0} \sum_{\mathbf{q}',j''} \delta(\mathbf{q}' - \bar{\mathbf{q}}) |V^{(3)}(\mathbf{q}, \mathbf{q}', j', \mathbf{q}'', j'')|^2 \\
 & \quad \times [(1 + n_{\mathbf{q}',j'} + n_{\mathbf{q}'',j''}) \delta(\hbar\omega_{\mathbf{q},j} - \hbar\omega_{\mathbf{q}',j'} - \hbar\omega_{\mathbf{q}'',j''}) \\
 & \quad + 2(n_{\mathbf{q}',j'} - n_{\mathbf{q}'',j''}) \delta(\hbar\omega_{\mathbf{q},j} + \hbar\omega_{\mathbf{q}',j'} - \hbar\omega_{\mathbf{q}'',j''})].
 \end{aligned} \tag{6}$$

We plot the resulting $[\tau^{\mathbf{q},j,j'}(\bar{\mathbf{q}})]^{-1}$ inside the Brillouin zone, with different color depending on j' . We have examined this decomposition for GaAs at 50 K, to study the attenuation of the LA phonons at 150 GHz, where the Herring processes dominate the scattering, and at 900 GHz, where Herring's processes have become the minority. The isosurfaces are color-coded depending on the band number of the final state.

In particular, the yellow and red surfaces contain the $\hbar\mathbf{q}$ vectors responsible for Herring's scattering. We can see how at low energy, along [100] [Fig. 4(a)] the picture is consistent with the Herring model, with most of the scattering events occurring along the [100] direction (the red volume), with also an important amount of scattering around the [111] directions

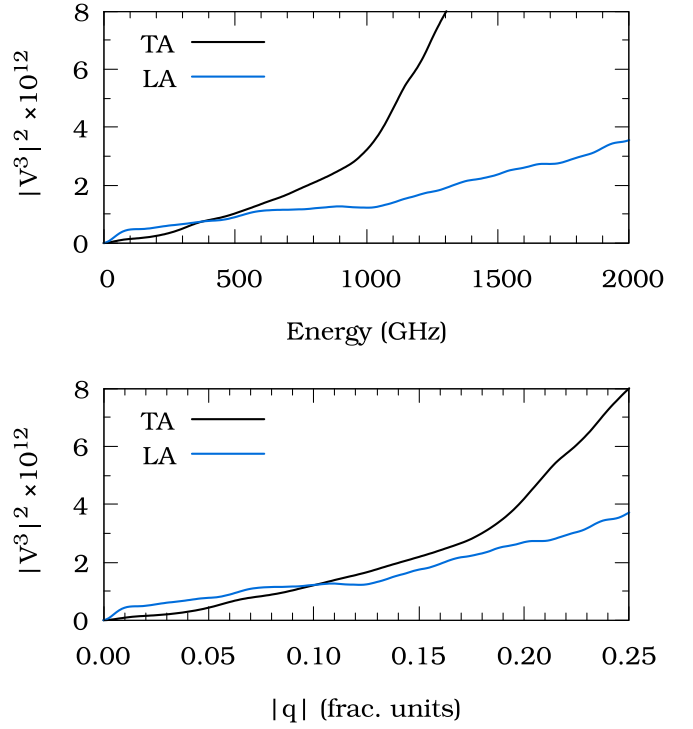


FIG. 5. GaAs, [100] direction. Squared matrix element involved in the scattering of the initial longitudinal (black line) and transverse (blue line) phonons, averaged over the BZ with respect to the \mathbf{q}' wave vector, represented as a function of the q_x component of the initial \mathbf{q} wave vector (lower panel) and initial phonon frequency (upper panel).

(the yellow volumes). A significant fraction of the Brillouin zone (BZ) (around 14% of the BZ volume) is actively participating in the scattering. However, at the same energy but along the [111] direction [panel (c)], only a smaller volume around [111] and some small pockets close to the surface of the BZ in direction [100] are Herring active (about 4% of the BZ volume). One sees in Fig. 2 by how much the attenuation at 150 GHz is smaller along [111] than along [100]. In panels (b) and (d) of Fig. 4, we can see that as we move toward higher energies of the initial phonon, the scattering mechanisms become more complex, and they involve all the bands (including the longitudinal band, in green) and entail large chunks of the BZ.

3. Average matrix element

The importance of the effect of the matrix elements is illustrated in Fig. 5, where we report the average value of $|V^{(3)}|^2$ involved in the scattering process of the LA and TA phonons along the [100] direction of GaAs, as a function of phonon frequency and wave vector. One can see that the value is almost linear at low energy for TA phonons, but deviates from linearity around 1000 GHz, becoming more steep. For LA phonons, on the contrary, the behavior of the average matrix element is not linear even below 1000 GHz, and exhibits, after an initial growth, a saturation between 600 and 1000 GHz, followed by a rapid increase above 1000 GHz, when processes other than the Herring one start to dominate

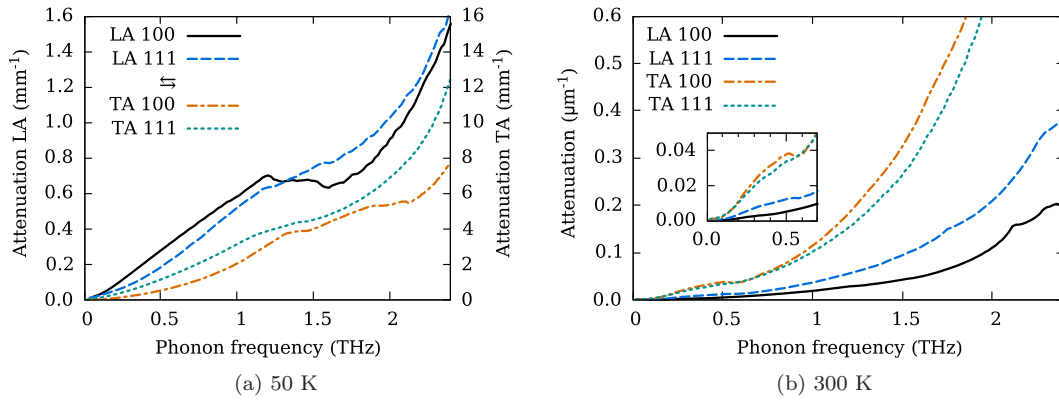


FIG. 6. Silicon. Attenuation of the longitudinal and transverse acoustic phonons along the [100] and [111] directions at 50 K (left panel) and 300 K (right panel). Note the change of scale between the two temperatures (panels), as well as the different axis (on the right) for the TA mode in the left panel.

the scattering. The convolution of $|V^{(3)}|^2$ with the T-JDOS explains most of the shape of the attenuation in functions of ω , with the sharp features being imputable to the complex interplay between the matrix-element magnitude and the overlap of phonon polarizations, which are inherent to the definition [31] of $V^{(3)}$.

V. RESULTS FOR SILICON

In Fig. 6, we report the computed attenuation of LA and TA phonons along the [100] and [111] directions at 50 and 300 K. At low temperature [panel (a)], there is a visible plateau in the LA and TA branches along the [100] direction between 1.2 and 1.7 THz. When we examine the [111] direction, as in the case of GaAs, the plateau is not as pronounced as in the [100] direction. Nonetheless, a change of behavior is clearly visible in the same energy range as in the [100] direction.

At room temperature [panel (b)], the curves look smooth in the terahertz region. However, a careful examination re-

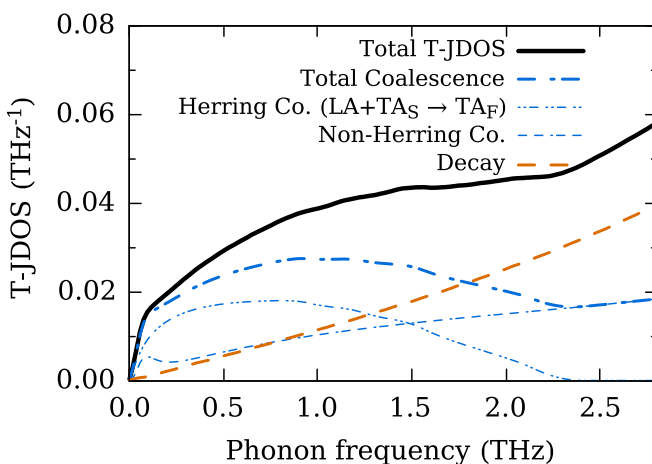


FIG. 7. Temperature-dependent joint density of states (T-JDOS) at 50 K for the LA branch of silicon along the [100] direction. The total T-JDOS (thick black solid line) is decomposed into decay (dashed orange) and coalescence (dot-dashed blue) processes, the latter being further divided into Herring's (LA \rightarrow TA_S + TA_F, blue dash-dotted lines) and non-Herring's (blue long-dashed lines) processes.

veals the presence of a small plateau, or a shoulder, around 500 GHz, which is magnified in the inset of Fig. 6(b).

We conclude that our theoretical results predict a plateau for the attenuation of the LA [100] phonon between 1.2 and 1.7 THz, similar to the one which is found in GaAs both experimentally and theoretically.

To the best of our knowledge, there is no experimental data available for the attenuation of acoustic waves in silicon in the range of frequencies for which we predict the attenuation plateau. There are few experimental results of sound absorption in silicon for frequencies above 10 GHz [24,26,53]. In Ref. [24], data have been obtained in the 50–100 GHz frequency and 30–130 K temperature ranges. As explained in the Introduction, such conditions correspond to an intermediate regime coming from the transition between the LR regime and the Akhiezer one, where the collective behavior of the phonon gas comes into play. The study of the intermediate regime is beyond the scope of the present work.

In analogy to what we have seen for GaAs in Sec. IV D 1, we examine in Fig. 7 the T-JDOS of silicon. Herring's mechanism dominates in a frequency range similar to the one in GaAs, up to 1 THz; however, the T-JDOS has a shorter and steeper onset and a larger saturation area, and it dies off slower than in GaAs, around 2.4 THz. This difference with respect to GaAs is consistent with the higher values of the phonon energy and group velocity of silicon. As a consequence, at low temperatures, the plateau spans a larger energy range than in GaAs, and should be observable.

At 300 K (results not shown in the main text), the weight of scattering processes involving high-energy phonons increases: a small plateau is visible around 500 MHz, and can be associated with the initial high steepness of the Herring T-JDOS. On the other hand, at 300 K, the large maximum of Herring's mechanism is not sufficiently steep to appear in the total attenuation curve, unless a careful examination is performed, as done in the inset of Fig. 6(b).

VI. GENERALIZATION TO OTHER CUBIC SEMICONDUCTORS

We have presented in detail how the breakdown of the Herring scattering model produces a plateau or a shoulder,

and discussed the conditions of their observation in measurements of the attenuation α for two specific materials. In the following, we explain that it is a common feature of cubic semiconductors.

Indeed, Herring's model requires that the LA phonon along the [100] direction coalesces with a nondegenerate TA phonon into another TA phonon, the main regions that are active in the mechanisms are around the [100] and [111] directions (Fig. 4), with the former giving the main contribution at very low frequencies. The model assumes that all three phonon energies linearly depend on their wave vector: $\omega_\nu = A_\nu |\mathbf{q}_\nu|$ ($\nu = \text{LA, TA}_s, \text{TA}_f$). As a result, it is always possible to find a coalescence channel, as the phase space is proportional to $|\mathbf{q}|^2$. However, in order to have $\omega_{\text{LA}} + \omega_{\text{TA}_s} = \omega_{\text{TA}_f}$, the two TA phonons have to be at an energy higher than LA, and they quickly exceed the region where their dispersion is linear. The linear regime is in general quite limited in cubic semiconductors, up to $|q| \simeq 0.2\text{--}0.3$ inverse lattice units, in Si and GaAs.

A similar and complementary geometric argument holds for the main non-Herring decay process, $\omega_{\text{LA}} = \omega_{\text{TA}_{\text{fast}}} + \omega_{\text{TA}_{\text{slow}}}$: the phase space for decay is initially very small, being limited by energy conservation, and increases with ω_{LA} .

The total attenuation is initially the sum of two curves, and its behavior is an interplay between the two contributions: the Herring coalescence one that increases, saturates, and then decreases; and the non-Herring decay one, that increases from zero. It is clear that because of the different behaviors, a plateau will form, although its exact energy range and amplitude depend on the specific material, and can be predicted, as we show in the present work, by *ab initio* calculations.

VII. MODEL BASED ON ELASTIC CONSTANTS

It is worth noting that the information about the behavior of the phonon-phonon matrix elements discussed above, can be used to evaluate the applicability range of models used in the past [32–34] to describe the phonon-phonon interaction in materials. In these models, phonon-phonon matrix elements are described via linear combinations of elastic constants, and are linearly proportional to the phonon wave vectors of the three phonons involved in the interaction process (see Appendix for details). As one can see from Fig. 5, the behavior of the average of the matrix elements for phonon-phonon interaction starts to deviate more and more from linearity for both transverse and longitudinal phonons as the modulus of the wave vector grows. We have shown above in Fig. 4 that the phonons involved in three-phonon scattering processes responsible for acoustic wave attenuation can have wave vectors close to the BZ boundary. Indeed, it was shown in an earlier work [30] that it is impossible to reproduce the experimentally observed plateau in the attenuation of the LA [100] phonon in GaAs using the unmodified model based on elastic constants for the phonon-phonon interaction matrix elements. However, it was also shown in Ref. [30] that if the model for the phonon-phonon interaction matrix element was modified to account for saturation of the matrix elements (with an adjustable parameter), and the *ab initio* phonon dispersion was used, then the plateau could be reproduced, as shown

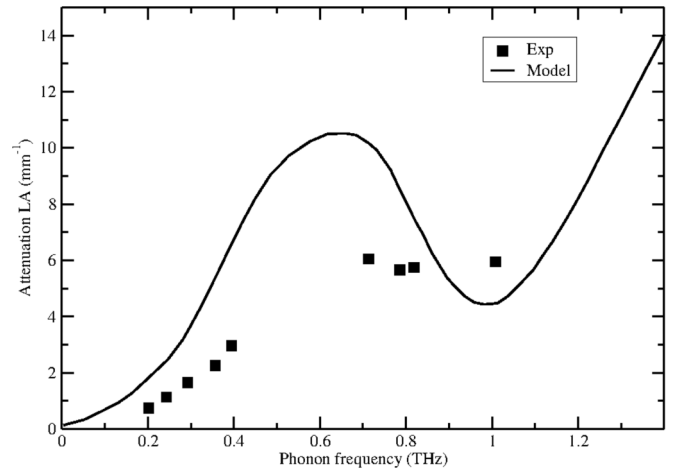


FIG. 8. GaAs at 50 K. Lines: attenuation of LA phonon obtained in Ref. [30] with a modified model based on elastic constants and *ab initio* phonon dispersion (see text). Symbols: experimental data of Ref. [27].

in Fig. 8. Indeed, the qualitative similarity of the theoretical results obtained in Ref. [30] with a (modified) model based on elastic constants and *ab initio* phonon dispersion, shown in Fig. 8, to the ones presented in this work in Fig. 2, highlights once again the fact that the plateau is due to the interplay between T-JDOS (which is determined solely by the phonon dispersion) and the phonon-phonon matrix elements. One must note, however, that quantitatively, the fully *ab initio* results of Fig. 2 agree much better with experimental data than the ones presented in Fig. 8. The details of the model proposed in work [30] are described in the Appendix.

VIII. CONCLUSIONS

We have computed within density functional perturbation theory the intrinsic phonon-phonon scattering processes for the very low frequency region of crystalline gallium arsenide and silicon phonon dispersion. For GaAs we have compared the calculations along the [100] direction with experiments, finding the agreement to be excellent, both as a function of the phonon frequency, at constant temperature, and as a function of temperature, for a given phonon frequency.

We are able to give some insight into the mechanisms underlying the anomalous, but quite general, appearance of a plateau (especially for the LA phonon) or shoulder (for TA) in the phonon attenuation as a function of frequency, appearing between 600 GHz and 1 THz for GaAs, and between 1.2 and 1.7 THz for silicon.

Specifically, the plateau is caused by the three-phonon coalescence Herring processes, which dominate at low frequency, progressively saturating and then rapidly decreasing as the states involved in the scattering move up in energy, over the limit of the acoustic part of the phonon dispersion. The saturation is caused by the acoustic phonon dispersion changing from linear to constant at low energy, which is a common feature of cubic semiconductors.

One of the major consequences of the breakdown of Herring's processes is that the absorption length of

longitudinal acoustic waves at 1 THz in semiconductors could be pretty large even at room temperature (50 μm at 300 K in silicon for a wavelength of 8.5 nm), opening interesting possibilities for high-resolution phonon imaging of deeply embedded nanostructures.

It is interesting to observe that the magnitude of the attenuation can be quite different for different directions and branches, but the plateau is still present grossly in the same frequency range. On the other hand, it becomes less visible at higher temperatures as more scattering channels involving the optical bands reduce the dominance of the simple Herring decay mechanism, drowning it out at lower frequencies.

ACKNOWLEDGMENTS

This work was granted HPC resources of IDRIS, CINES, and TGCC under the GENCI Projects 7320 and 2210, and by the Ecole Polytechnique through the LLR-LSI project. We acknowledge support from the Chaire Énergie of the École Polytechnique.

APPENDIX

We briefly present the model for the anharmonic coefficients and its modification proposed in Ref. [30].

In the long-range approximation, the phonon-phonon matrix element can be written as [34]

$$V^{(3)}(\mathbf{q}j, \mathbf{q}'j', \mathbf{q}''j'') = \frac{\Phi(\mathbf{q}j, \mathbf{q}'j', \mathbf{q}''j'')}{\omega_j \omega_{j'} \omega_{j''}}, \quad (\text{A1})$$

with

$$\begin{aligned} \Phi(\mathbf{q}j, \mathbf{q}'j', \mathbf{q}''j'') &= \sum_{\alpha\beta\gamma\delta\mu\nu} \mathbf{S}_{\alpha\beta,\gamma\delta,\mu\nu} \times \mathbf{q}_{j,\alpha} \mathbf{q}'_{j',\gamma} \mathbf{q}''_{j'',\mu} \times \mathbf{e}_{j,\beta} \mathbf{e}'_{j',\delta} \mathbf{e}''_{j'',\nu}, \\ \mathbf{S}_{\alpha\beta,\mu\nu,\zeta\xi} &= \mathbf{C}_{\alpha\beta,\mu\nu,\zeta\xi} + \delta_{\alpha\mu} \mathbf{C}_{\beta\nu,\zeta\xi} + \delta_{\alpha\zeta} \mathbf{C}_{\mu\nu,\beta\xi} + \delta_{\mu\zeta} \mathbf{C}_{\alpha\beta,\nu\xi}, \end{aligned} \quad (\text{A2})$$

where \mathbf{C} stands for both the second- and third-order tensors of elastic constants and \mathbf{e} are the phonon polarizations. As one can see, the linear dependence on the \mathbf{q} vectors of the three phonons involved in the interaction is built in the model of Ref. [34]. Thus, the model cannot describe the saturation of phonon frequencies and phonon-phonon matrix elements for phonon wave vectors far from the center of the Brillouin zone.

In order to take the saturation into account, a simple modification was proposed in Ref. [30]:

$$\begin{aligned} \Phi(\mathbf{q}j, \mathbf{q}'j', \mathbf{q}''j'') &= \sum_{\alpha\beta\gamma\delta\mu\nu} \mathbf{S}_{\alpha\beta,\gamma\delta,\mu\nu} \times \tilde{\mathbf{q}}_{j,\alpha} \tilde{\mathbf{q}}'_{j',\gamma} \tilde{\mathbf{q}}''_{j'',\mu} \times \mathbf{e}_{j,\beta} \mathbf{e}'_{j',\delta} \mathbf{e}''_{j'',\nu}, \quad \tilde{\mathbf{q}} = \begin{cases} \mathbf{q} & \text{if } |\mathbf{q}| < q_c \\ q_c \cdot \frac{\mathbf{q}}{|\mathbf{q}|} & \text{if } |\mathbf{q}| \geq q_c, \end{cases} \\ \mathbf{S}_{\alpha\beta,\mu\nu,\zeta\xi} &= \mathbf{C}_{\alpha\beta,\mu\nu,\zeta\xi} + \delta_{\alpha\mu} \mathbf{C}_{\beta\nu,\zeta\xi} + \delta_{\alpha\zeta} \mathbf{C}_{\mu\nu,\beta\xi} + \delta_{\mu\zeta} \mathbf{C}_{\alpha\beta,\nu\xi}. \end{aligned} \quad (\text{A3})$$

As one can see, the matrix elements are now allowed to grow linearly with \mathbf{q} only until the \mathbf{q} vector reaches a “saturation wave vector” q_c . In Ref. [30], q_c was treated as a fitting parameter, which we found to be $q_c = 0.37(\frac{2\pi}{a_0})$ for GaAs, for all the temperatures and all initial acoustic phonon frequencies considered.

-
- [1] J. W. Tucker and V. W. Rampton, *Microwave Ultrasonics in Solid State Physics* (North-Holland, Amsterdam, 1972).
 - [2] H. E. Bommel and K. Dransfeld, *Phys. Rev. Lett.* **2**, 298 (1959).
 - [3] W. P. Mason and T. B. Bateman, *J. Acoust. Soc. Am.* **36**, 644 (1964).
 - [4] M. Pomerantz, *Phys. Rev.* **139**, A501 (1965).
 - [5] R. I. Cottam and G. A. Saunders, *J. Phys. C* **7**, 2447 (1974).
 - [6] J. Hasson and A. Many, *Phys. Rev. Lett.* **35**, 792 (1975).
 - [7] E. Chávez-Ángel, R. A. Zarate, J. Gomis-Bresco, F. Alzina, and C. M. S. Torres, *Semicond. Sci. Technol.* **29**, 124010 (2014).
 - [8] L. P. Zeng, K. C. Collins, Y. J. Hu, M. N. Luckyanova, A. A. Maznev, S. Huberman, V. Chiloyan, J. W. Zhou, X. P. Huang, K. A. Nelson, and G. Chen, *Sci. Rep.* **5**, 17131 (2015).
 - [9] X. Shi, L. Chen, and C. Uher, *Int. Mater. Rev.* **61**, 379 (2016).
 - [10] D. A. Broido, M. Malorny, G. Birner, N. Mingo, and D. A. Stewart, *Appl. Phys. Lett.* **91**, 231922 (2007).
 - [11] N. Mingo, D. Hauser, N. Kobayashi, M. Plissonnier, and A. Shakouri, *Nano Lett.* **9**, 711 (2009).
 - [12] T. F. Luo, J. Garg, J. Shiomi, K. Esfarjani, and G. Chen, *Europhys. Lett.* **101**, 16001 (2013).
 - [13] K. Esfarjani, G. Chen, and H. Stokes, *Phys. Rev. B* **84**, 085204 (2011).
 - [14] G. Fugallo, M. Lazzeri, L. Paulatto, and F. Mauri, *Phys. Rev. B* **88**, 045430 (2013).
 - [15] M. Markov, J. Sjakste, G. Fugallo, L. Paulatto, M. Lazzeri, F. Mauri, and N. Vast, *Phys. Rev. B* **93**, 064301 (2016).
 - [16] B. C. Daly, N. C. R. Holme, T. Buma, C. Branciard, T. B. Norris, D. M. Tennant, J. A. Taylor, J. E. Bower, and S. Pau, *Appl. Phys. Lett.* **84**, 5180 (2004).
 - [17] A. Fainstein, N. D. Lanzillotti-Kimura, B. Jusserand, and B. Perrin, *Phys. Rev. Lett.* **110**, 037403 (2013).
 - [18] G. Rozas, M. F. Pascual Winter, B. Jusserand, A. Fainstein, B. Perrin, E. Semenova, and A. Lemaître, *Phys. Rev. Lett.* **102**, 015502 (2009).
 - [19] M. Hamoumi, P. E. Allain, W. Hease, E. Gil-Santos, L. Morgenroth, B. Gérard, A. Lemaître, G. Leo, and I. Favero, *Phys. Rev. Lett.* **120**, 223601 (2018).

- [20] C. Thomsen, H. T. Grahn, H. J. Maris, and J. Tauc, *Phys. Rev. B* **34**, 4129 (1986).
- [21] A. Huynh, B. Perrin, B. Jusserand, and A. Lemaitre, *Appl. Phys. Lett.* **99**, 191908 (2011).
- [22] P. A. Mante, Y. R. Huang, Y. Szu-Chi, T. M. Liu, A. A. Maznev, J. Sheu, and C. K. Sun, *Ultrasonics* **56**, 52 (2015).
- [23] A. Huynh, B. Perrin, and A. Lemaitre, *Ultrasonics* **56**, 66 (2015).
- [24] H. Y. Hao and H. J. Maris, *Phys. Rev. B* **63**, 224301 (2001).
- [25] J. Y. Duquesne and B. Perrin, *Phys. Rev. B* **68**, 134205 (2003).
- [26] B. C. Daly, K. Kang, Y. Wang, and D. G. Cahill, *Phys. Rev. B* **80**, 174112 (2009).
- [27] R. Legrand, A. Huynh, B. Jusserand, B. Perrin, and A. Lemaitre, *Phys. Rev. B* **93**, 184304 (2016).
- [28] H. Maris, in *Physical Acoustics*, edited by W. P. Mason (Academic Press, New York, 1971), Vol. 8, pp. 279–345.
- [29] C. Herring, *Phys. Rev.* **95**, 954 (1954).
- [30] R. Legrand, *Acoustique—étude et utilisation de nouvelles sources et transducteurs aux longueurs d’onde nanométriques*, Ph.D. thesis, Université Pierre et Marie Curie - Paris VI, France, 2014 .
- [31] L. Paulatto, F. Mauri, and M. Lazzeri, *Phys. Rev. B* **87**, 214303 (2013).
- [32] S. Simons, *Math. Proc. Cambridge Philos. Soc.* **53**, 702 (1957).
- [33] S. I. Tamura, *Phys. Rev. B* **31**, 2574 (1985).
- [34] A. Berke, A. P. Mayer, and R. K. Wehner, *J. Phys. C* **21**, 2305 (1988).
- [35] M. Calandra, M. Lazzeri, and F. Mauri, *Physica C (Amsterdam)* **456**, 38 (2007).
- [36] M. Lazzeri, M. Calandra, and F. Mauri, *Phys. Rev. B* **68**, 220509 (2003).
- [37] S. Baroni, S. de Gironcoli, A. D. Corso, and P. Giannozzi, *Rev. Mod. Phys.* **73**, 515 (2001).
- [38] A. Debernardi, S. Baroni, and E. Molinari, *Phys. Rev. Lett.* **75**, 1819 (1995).
- [39] M. Lazzeri and S. de Gironcoli, *Phys. Rev. Lett.* **81**, 2096 (1998).
- [40] M. Lazzeri and S. de Gironcoli, *Phys. Rev. B* **65**, 245402 (2002).
- [41] This derivative has to be done with some care, to avoid problems when phonon branches cross or are degenerate. Details can be found in Sec. IV of Ref. [14].
- [42] P. Giannozzi, S. Baroni, N. Bonini, M. Calandra, R. Car, C. Cavazzoni, D. Ceresoli, G. Chiarotti, M. Cococcioni, I. Dabo, A. Dal Corso, S. De Gironcoli, S. Fabris, G. Fratesi, R. Gebauer, U. Gerstmann, C. Gougousis, A. Kokalj, M. Lazzeri, L. Martin-Samos, N. Marzari, F. Mauri, R. Mazzarello, S. Paolini, A. Pasquarello, L. Paulatto, C. Sbraccia, S. Scandolo, G. Sclauzero, A. Seitsonen, A. Smogunov, P. Umari, and R. Wentzcovitch, *J. Phys.: Condens. Matter* **21**, 395502 (2009).
- [43] P. Giannozzi, O. Andreussi, T. Brumme, O. Bunau, M. B. Nardelli, M. Calandra, R. Car, C. Cavazzoni, D. Ceresoli, M. Cococcioni, N. Colonna, I. Carnimeo, A. D. Corso, S. de Gironcoli, P. Delugas, R. A. D. J. A. Ferretti, A. Floris, G. Fratesi, G. Fugallo, R. Gebauer, U. Gerstmann, F. Giustino, T. Gorni, J. Jia, M. Kawamura, H.-Y. Ko, A. Kokalj, E. Küçükbenli, M. Lazzeri, M. Marsili, N. Marzari, F. Mauri, N. L. Nguyen, H.-V. Nguyen, A. O. de-la Roza, L. Paulatto, S. Poncé, D. Rocca, R. Sabatini, B. Santra, M. Schlipf, A. P. Seitsonen, A. Smogunov, I. Timrov, T. Thonhauser, P. Umari, N. Vast, X. Wu, and S. Baroni, *J. Phys.: Condens. Matter* **29**, 465901 (2017).
- [44] J. P. Perdew and A. Zunger, *Phys. Rev. B* **23**, 5048 (1981).
- [45] J. P. Perdew, K. Burke, and M. Ernzerhof, *Phys. Rev. Lett.* **77**, 3865 (1996).
- [46] M. Fuchs and M. Scheffler, *Comput. Phys. Commun.* **119**, 67 (1999).
- [47] S. Botti, N. Vast, L. Reining, V. Olevano, and L. C. Andreani, *Phys. Rev. Lett.* **89**, 216803 (2002).
- [48] S. Botti, F. Sottile, N. Vast, V. Olevano, L. Reining, H.-C. Weissker, A. Rubio, G. Onida, R. Del Sole, and R. W. Godby, *Phys. Rev. B* **69**, 155112 (2004).
- [49] J. Sjakste, V. Tyuterev, and N. Vast, *Phys. Rev. B* **74**, 235216 (2006).
- [50] H. J. Monkhorst and J. D. Pack, *Phys. Rev. B* **13**, 5188 (1976).
- [51] A. J. Kent, N. M. Stanton, L. J. Challis, and M. Henini, *Appl. Phys. Lett.* **81**, 3497 (2002).
- [52] See Supplemental Material at <http://link.aps.org/supplemental/10.1103/PhysRevB.98.245201> for detailed figures for both materials, several temperatures, and several high-symmetry directions.
- [53] F. Hudert, A. Bruchhausen, D. Issenmann, O. Schecker, R. Waitz, A. Erbe, E. Scheer, T. Dekorsy, A. Mlayah, and J.-R. Huntzinger, *Phys. Rev. B* **79**, 201307 (2009).